Microporous and Mesoporous Materials 328 (2021) 111487

Contents lists available at ScienceDirect

Microporous and Mesoporous Materials

journal homepage: www.elsevier.com/locate/micromeso

Solventless synthesis of ZIF-L and ZIF-8 with hydraulic press and high temperature

Marta Pérez-Miana [a,b], Javier U. Reséndiz-Ordóñez [c], Joaquín Coronas [a,b,*]

[a] Instituto de Nanociencia y Materiales de Aragón (INMA), CSIC-Universidad de Zaragoza, 50018 Zaragoza, Spain
[b] Chemical and Environmental Engineering Department, Universidad de Zaragoza, 50018 Zaragoza, Spain
[c] Universidad Nacional Autónoma de México, México DF, Mexico

ARTICLE INFO

Keywords:
Solventless synthesis
High pressure
Metal organic framework
Zeolitic imidazolate framework
ZIF-8

ABSTRACT

In recent years, alternative methods to conventional synthesis of MOFs (metal-organic frameworks) have emerged due to the problematic use of solvents for both the environment and human health. Here we present the synthesis of ZIFs (zeolitic imidazolate frameworks) at high pressure by means of a hydraulic press provided with a heating mechanism. By the optimization of parameters such as temperature, time and the addition of promotor NH_4NO_3, a considerable increase in the reaction yield was achieved in products, neither washed nor activated, obtained since the first minute of reaction. Depending on the operation conditions, ZIF-L appeared as competing phase with ZIF-8. Upon transformation of ZIF-L into ZIF-8 in presence of ethanol, a reaction yield of 58.2% was achieved to highly crystalline ZIF-8 with a BET specific surface area of 947 m^2/g. This green, fast, versatile and improved method suggests a possible way to future synthesis of other MOFs and the possibility of their industrial implementation.

1. Introduction

MOFs (metal-organic frameworks) are versatile materials due to their use in a vast number of applications [1]. MOFs are organic-inorganic crystalline porous materials composed by an inorganic part (a metal cluster) joined by coordination bonds to organic ligands [2]. Among their very interesting properties, it should be highlighted the high and permanent porosity [3] and the possibility of changing the pore architecture and functionality [4,5], which can be achieved by the modification of the ligand. These properties make them suitable materials for use in applications such as catalysis [1], gas storage [3,6,7], membrane separation [8,9], drug delivery [10] and encapsulation [11,12], among others.

In this work we focus on the family of MOFs based on imidazolate ligands, the so-called ZIFs (zeolitic imidazolate frameworks) with tetrahedral coordination geometry. This name derives from the similarity of the angle formed by the metal ion and the ligands with that present in zeolites between aluminum or silicon and oxygen atoms: 145° [13]. Among the most prominent ZIFs, ZIF-8, a MOF with the SOD type structure, is composed of Zn metals coordinated to nitrogen atoms present in the organic ligand 2-methylimidazolate. ZIF-8 has micropores of 0.34 nm with cavities of 1.1 nm, high thermal stability (up to 400 °C) and a hydrophobic character [13]. This MOF has been widely studied for applications such as gas separation [14], encapsulation [15], H_2 storage [16] and catalysis [17].

The synthesis of these materials has usually been carried out mainly through solvothermal processes. However, due to the problem of using some solvents (especially during the synthesis but also in the following washing and activation processes), more respectful processes with environment and health have arisen. Examples of these new methods are hydrothermal processes [18], microwave-assisted synthesis [19], sonocrystallization [20], mechanosynthesis [21] and high-pressure synthesis [22]. These last two methods, besides having the advantage of avoiding solvents (and therefore potential contamination and high invest, as regards to solvents such as dimethylformamide, dimethylsulfoxide, etc.), they allow working in much shorter synthesis times than in case of solvothermal methods. These syntheses require a short time in the order of minutes instead of hours or even days as in the case of solvothermal ones, which is very interesting when thinking of scaling up to industrial productions.

Regarding the high pressure method, some previous studies dealt with the variation of pressure and its consequence on the structure of MOFs [23,24], while a previous solventless synthesis of ZIF-8 at high pressure and room temperature [22] and solventless high pressure

* Corresponding author. Instituto de Nanociencia y Materiales de Aragón (INMA), CSIC-Universidad de Zaragoza, 50018 Zaragoza, Spain.
E-mail address: coronas@unizar.es (J. Coronas).

https://doi.org/10.1016/j.micromeso.2021.111487
Received 28 May 2021; Received in revised form 5 October 2021; Accepted 6 October 2021
Available online 14 October 2021

encapsulation of several organic compounds in carboxylate type MOFs [25] were done in our laboratory. Here, the effect of temperature, time, ligand:metal ratio and the addition of promotor on high-pressure synthesis of ZIF-8 and ZIF-L will be analyzed. These parameters have not yet been studied and it is believed that can have a great effect on the characteristics of the final products and their reaction yield. It will also be the first time that the conversion of ZIF-L obtained from solventless high pressure method into ZIF-8 is studied.

2. Experimental section

2.1. Synthesis of ZIF-8

As base synthesis, we adapted the procedure that Paseta et al. [22] carried out in which stoichiometric amounts of metal and ligand were used (2:1 ligand:metal ratio), following the empirical formula Zn $(mIm)_2$, where mIm corresponds to 2-methylimidazolate. A hydraulic press was used for the solventless synthesis (YLJ 15T, MTI corporation). The press is provided with a thermal jacket (500 W) which wraps the cylinder where the reaction takes place, as shown in Fig. 1. The operating pressure along the study was in the 60–600 MPa range.

Fig. 1 shows a scheme of the inner part of the press. In the middle, the cylinder where the reaction takes place. Inside it, a short rod has the function of base where the solid reactants are placed. After inserting the reactants, the upper rod is introduced, which acts as piston. Surrounding the reaction cylinder, there is another concentric cylinder, which is provided with a heating mechanism connected to a controlling system (Fig. S1). The operating temperature was in the 20–145 °C range.

The base synthesis consists of 0.203 g of ZnO (2.5 mmol; Sigma-Aldrich, ≥99%) placed in a vial (8 mL) with 0.410 g of Hmlm (5 mmol; Acros-Organics, 99%) and mixed by hand shaking for about 2 min. The mixture was then placed inside the metal cylinder of the hydraulic press previously heated up to the reaction temperature (room temperature, 70, 90, 110, 130 and 145 °C). Then, the mixture was compacted under different pressures (60, 150, 240, 300, 450 and 600 MPa) and times (1, 2, 5, 10, 20, 60 and 240 min). After that, the obtained pills were analyzed directly, without washing or purifying, since the contact with any solvent may promote the reaction between the excess reactants.

Similarly, the procedure was repeated with different mIm:Zn molar ratios (from 2:1 to 3:1) and with the addition of different amounts of NH_4NO_3 (5, 10, 15, 20, 40 and 80 mg e.g. 0.8–11.6 wt% to the total content of reactants) to the synthesis solid mixture for increasing the reaction yield.

For comparison, ZIF-8 was synthesized through a conventional solvothermal method [15]. Two solutions were prepared with methanol as solvent. For the first one, 6.85 g (83 mmol) of HmIm (Acros-Organics, 99%) was dissolved in 200 mL of methanol. For the second one, 2.93 g (9.8 mmol) of $Zn(NO_3)_2{\cdot}6H_2O$ (Sigma-Aldrich, 98%) was dissolved in 200 mL of methanol. Both solutions were mixed and stirred during 30 min at room temperature. The suspension obtained was centrifuged at 8000 rpm for 15 min. The solid recovered was washed twice with 15 mL of methanol, centrifuged under the same conditions and dried at room temperature overnight.

2.2. Characterization

X-ray diffraction (XRD) was performed at room temperature by powder X-ray diffractometry (PXRD, Bruker D8 Advance) with a copper anode and a graphite monochromator to select Cu Kα radiation with $\lambda = 1.5418$ Å. Data were gathered in the 2θ range = 5−40°, and the scanning rate was 0.03°/s.

Thermogravimetric analyses (TGA) were carried out using Mettler Toledo TGA/SDTA 851e equipment. The samples were put in 70 μL alumina pans and heated up to 700 °C with a heating rate of 10 °C/min under air atmosphere. The yield was calculated from the TGA data as the quotient between grams of ZnO in ZIF-8 and total grams of ZnO in the sample (Equation (1)). The ZnO yield to ZIF-8 was estimated from the stoichiometric formula, $Zn(mIm)_2$, considering ZnO and mIm in dry basis in pure ZIF-8. Unreacted ligand and solvent was discounted, i.e. the TGA mass loss in % below 350 °C was discarded and this value at around 350 °C (i.e. *mIm in sample* in equation (1)) was normalized to 100% of the total loss of mass. 33.69 and 66.31 g are the amounts of ZnO and mIm respectively calculated in 100 g of ZIF-8.

$$Yield\ (\%) = \frac{mIm\ in\ sample\ (\%) \cdot \frac{33{,}69\ g\ ZnO\ in\ ZIF-8}{66{,}31\ g\ mIm\ in\ ZIF-8}}{(100 - mIm\ in\ sample\ (\%))\ g\ ZnO\ in\ sample} \cdot 100 \qquad \text{Equation 1}$$

Scanning electron microscopy (SEM) was performed using an Inspect-F microscope (FEI) operated at 10 kW. The samples were prepared over a magnetic strip by coating with gold under vacuum conditions.

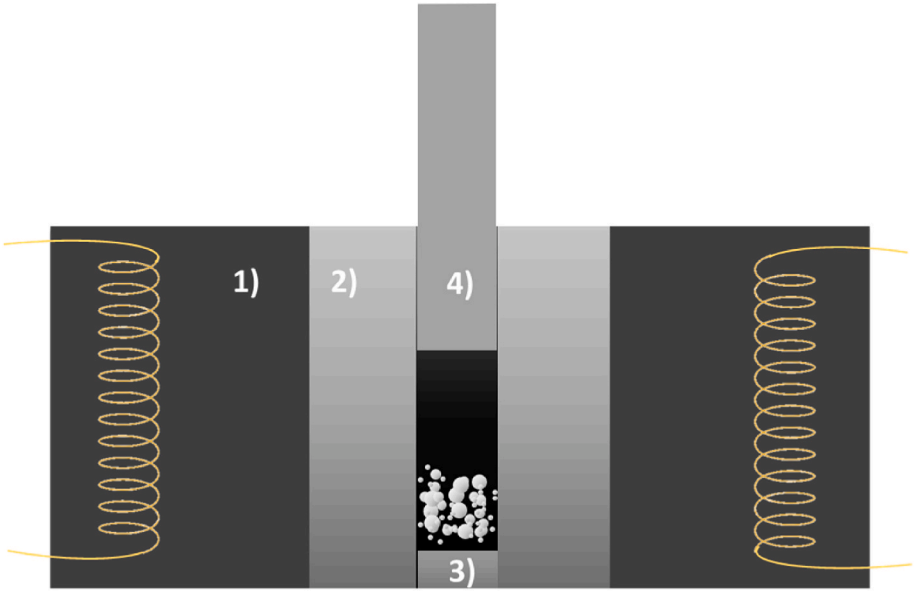

Fig. 1. *Scheme of the cross section of the press.* 1 – Heating cylinder, 2 - steel sleeve (die) or cylinder with 1.27 cm ID and 10.0, cm length, 3 – pushing rod (downer one/base), 4 – pushing rod (upper one/piston).

Nitrogen adsorption−desorption isotherms were performed using Micrometrics Tristar 3000 with N_2 at 77 K. The samples were outgassed under vacuum for 8 h at 200 °C. The Brunauer−Emmett−Teller (BET) method was applied to calculate the BET specific surface area.

3. Results and discussion

In this work, we demonstrate that an improvement of the solventless synthesis of ZIFs at high pressure is possible by increasing temperature and adding a promotor, in our case NH_4NO_3. Synthesis of ZIF-8 was carried out by working with a press provided with a heating unit. The main advantage of the high pressure method as compared to the other solid state method of mechanosynthesis [26] is the avoidance of grinding and its consequent effect on particle size and shape and possible amorphization. For the synthesis of ZIF-8, ZnO was used as Zn source, following the demonstration of its reactivity by mechanosynthesis [21,26–28]. Paseta et al. already tried with different Zn salt for high pressure method and they did not observe apparent reaction when Zn nitrate, acetate and chloride salts were used (after washing with ethanol the solids they obtained at high pressure were totally dissolved) [22]. However, we tried with Zn nitrate at high temperature conditions to check if temperature promoted the reaction but it did not work either. $Zn(acetilacetonate)_2$ was also tried to check another option of Zn salt but any sign of reaction was realized in terms of TGA data and XRD analysis. They were also discarded due to problems with possible formation of acids (HCl, HNO_3, HAc, …) and corrosion of the press.

Different conditions of time, temperature, ligand:metal ratio and amount of promotor were studied. For choosing the best conditions of each parameter, characterization studies were made in samples neither washed nor activated and yields were calculated from TGA data in air as

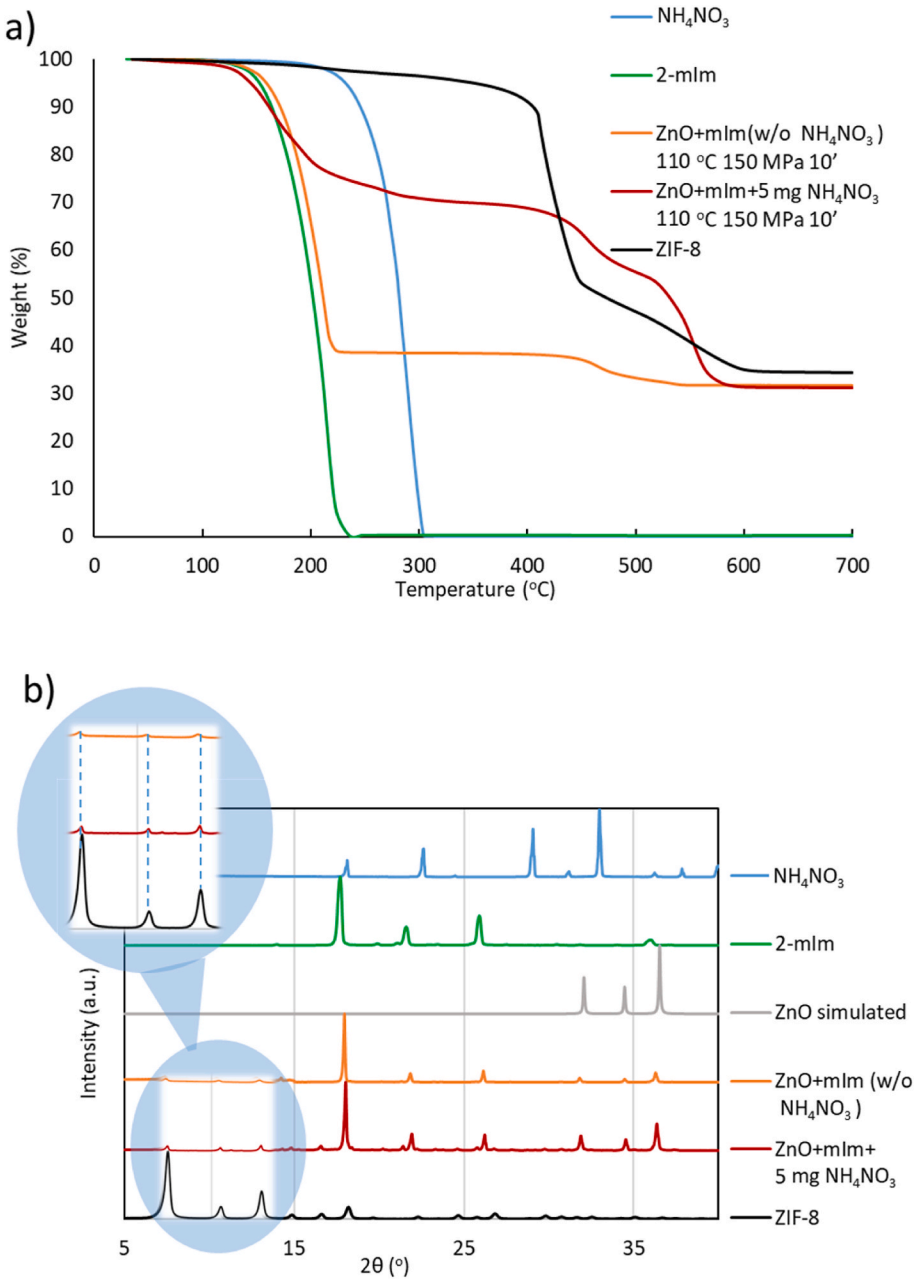

Fig. 2. a) TGA curves of the salt, ligand, ZIF-8 from a solvothermal synthesis and from syntheses both with and without NH_4NO_3. b) XRD patterns of the salt, ligand, ZIF-8 from a solvothermal synthesis and from solventless syntheses both with and without NH_4NO_3; the inset shows intensities from 5 to 15° multiplied by 10 in the solventless syntheses without salt.

explained in the experimental section.

3.1. Addition of NH_4NO_3

As an overview, Fig. 2a shows the normalized weight losses from the TGA of the main compounds involved in this study as well as the desired product, ZIF-8, when synthesized by conventional solvothermal conditions (with methanol) and by high pressure method with and without the addition of NH_4NO_3. This salt was used because an increase on the reaction yield was reported with its addition at room temperature solventless conditions [22,26]. Similarly to the procedure that Tanaka et al. reported in 2018 for the mechanosynthesis of ZIF-8 [26], here, the acid character of NH_4^+ from NH_4NO_3 promotes the acid dissolution of ZnO (Equation (2)). Generated NH_3 will deprotonate HmIm (Equation (3)), which will react with ionized Zn forming ZIF-8 (Equation (4)).

$$ZnO + 2NH_4NO_3 \rightarrow Zn^{2+} + 2NH_3 + H_20 + 2NO_3^- \quad \text{Equation 2}$$

$$NH_3 + HmIm \rightarrow NH_4^+ + mIm^- \quad \text{Equation 3}$$

$$Zn^{2+} + 2mIm^- \rightarrow Zn(mIm)_2 \quad \text{Equation 4}$$

NH_3/NH_4^+ catalyze the formation of ZIF-8. An increased amount of NH_4NO_3, could promote the formation of ZIF-L phase due to the formation of H_20 molecules, which are present in the formula of this phase: $Zn(mlm)_2{\cdot}(HmIm)_{1/2}{\cdot}(H_2O)_{3/2}$ [29]

Weight losses of this salt and of the ligand are also shown in order to check their decomposition temperatures, at around 220 and 145 °C, respectively. This temperature of 145 °C in TGA as well as 18, 22 and 26° intensities in the corresponding XRD patterns (Fig. 2b) from the synthesis through the high pressure method evidence that not all the ligand reacts when carrying out this method, even if a stoichiometric mIm/Zn molar ratio (2) was applied. On the other hand, all samples showed a fall in weight loss at around 465 °C, which corresponds to the decomposition temperature of ZIF-8. This can be considered as an evidence of reaction between Zn ion and the ligand (even though they were not washed). Moreover, the XRD patterns in Fig. 2b reveal that when adding NH_4NO_3 the ZIF-8 reflections increase appreciably. It should be noted that in the synthesis without salt, ZIF-8 was also formed. The amount of ZIF was obtained from the degradation temperature of ZIF-8 in TGA (Fig. 2a). On the other hand, XRD peaks (Fig. 2b) provide information of the crystallinity of this product, which is in agreement with TGA and confirms that ZIF-8 is achieved even if the peaks of unreacted ligand and ZnO predominate due to the low yield of that first and orientate reaction. To enhance the sensibility of the technique, the intensities from 5 to 15° were multiplied by 10 due to the low yield of this sample. XRD pattern of simulated ZnO is also collected in Fig. 2b in order to show the decrease in 32, 34, 37° intensities as far as the yield to ZIF increases. These intensities do not disappear completely in any case due to the fact that ZnO did not react completely remaining in part in the final product.

3.2. Effect of temperature

Different reaction temperatures were analyzed before studying the addition of NH_4NO_3 in order to elucidate how it affects to the characteristics of the products, particularly in what concerns the ZIF yield. As Table 1 depicts, the highest yield of 5.8% was obtained at 145 °C (run #6 in Table 1), temperature at which the ligand starts to melt. To avoid the melting of reactants while working with the press and also possible ligand emanations, the second highest yield of 4.6% obtained at 110 °C (run #4 in Table 1) was considered to fix this variable and to continue with the optimization of the other parameters. TGA data and XRD

Table 1
Yields calculated from TGA data for the different conditions analyzed. Run #8 was repeated four times.

RUN		Temperature (°C)	Pressure (MPa)	NH_4NO_3 (mg)	Time (min)	L/M ratio	Yield (%)
#1	Different temperature	20	300	0	10	2	2.4
#2		70	300	0	10	2	3.2
#3		90	300	0	10	2	3.4
#4		**110**	300	0	10	2	4.6
#5		130	300	0	10	2	4.0
#6		145	300	0	10	2	5.8
#7	Different pressure	110	60	5	10	2	28.9
#8		110	**150**	5	10	2	32.8 ± 1.4
#9		110	240	5	10	2	30.2
#10		110	300	5	10	2	30.5
#11		110	450	5	10	2	29.7
#12		110	600	5	10	2	33.8
#13	Different amount of NH_4NO_3	110	150	5	10	2	32.0
#14		110	150	10	10	2	35.1
#15		110	150	**15**	10	2	40.2
#16		110	150	20	10	2	39.4
#17		110	150	**40**	10	2	57.5
#18		110	150	80	10	2	54.7
#19	Different reaction time (40 mg NH_4NO_3)	110	150	40	1	2	43.0
#20		110	150	40	2	2	38.1
#21		110	150	40	5	2	39.0
#22		110	150	40	**10**	2	57.5
#23		110	150	40	20	2	38.7
#24		110	150	40	240	2	47.4
#25	Different reaction time (15 mg NH_4NO_3)	110	150	15	1	2	34.9
#26		110	150	15	2	2	35.6
#27		110	150	15	5	2	33.9
#28		110	150	15	**10**	2	40.2
#29		110	150	15	20	2	35.4
#30		110	150	15	60	2	35.8
#31		110	150	15	240	2	38.8
#32	Different mIm/Zn ratio (40 mg NH_4NO_3)	110	150	40	10	**2**	57.5
#33		110	150	40	10	2.5	33.2
#34		110	150	40	10	3	34.0
#35	Different mIm/Zn ratio (15 mg NH_4NO_3)	110	150	15	10	**2**	40.2
#36		110	150	15	10	2.5	34.7
#37		110	150	15	10	3	36.7

patterns (Fig. S2 and Fig. 3, respectively) show the loss of weight at 465 °C and intensities at 7.5, 10.5, 13 and 14°, which confirms the presence of ZIF-8 but with relatively low yield (intensities from 5 to 15° were also multiplied by 10 in solventless syntheses). Linker and ZnO are still appearing because those samples are neither washed nor activated. Even if the yield is increasing with temperature, we did not achieve yields of 100% and as products are not washed, unreacted compounds still remain in the sample.

3.3. Effect of pressure

The second parameter studied was the pressure (runs #7 to #12 in Table 1) exerted by the hydraulic press in the range from 60 MPa to 600 MPa. For this study, the temperature was fixed at 110 °C and 5 mg of NH_4NO_3 (0.8 wt%) was added to ZnO before mixing with ligand HmIm. The best results in terms of reaction yield were achieved at 600 MPa. Fig. S3 shows the corresponding XRD patterns and TGA curves. Both characterization techniques confirmed the presence of ZIF-8 in the terms above discussed. It is worth mentioning that one of the experiments (run #8 in Table 1) was repeated four times in order to obtain an average value with its standard deviation (32.8 ± 1.4% yield). This demonstrates the reliability and reproducibility of the approach followed in this study. In addition, it also confirms that the effect of pressure beyond 150 MPa (with reaction yield values in the 30–33% range at 150–600 MPa can be considered within the experimental error. Thus the pressure was fixed at 150 MPa for further experiments, a value easier to handle.

As complement, the influence of working pressure was also studied in a ZIF-8 previously synthesized by conventional solvothermal method with methanol. ZIF-8 was submitted to the same conditions of temperature and pressure (110 °C and 150 MPa) and there was an evidence in the distortion of the structure and a lost in the crystallinity. In consequence, the material showed a decrease in the BET specific surface area (from 1730 to 1074 m^2/g, see Table S1) as well as a less sharp shape in the XRD pattern and a slightly different weight loss curve (see Figs. S4a and S4b), which could be associated to the compactness of ZIF-8 with some cross-linking between the particles in the generated pellet. This change can also be appreciated in the derivatives of the TGA curves in Fig. S4c.

Furthermore, some experiments were performed in absence of pressure but at high temperature in order to elucidate their influences. Two different methods were carried out inside the press already heated: one of them consisted of just introducing the solid reactants (previously mixed by hand shaking) in the press, without using the piston; and in the other case, the piston was used to compact the previously hand shaken reactants but compacting just with the minimum pressure so that the manometer of the press did not detect a pressure change. Fig. S5a (TGA) and S5b (XRD) reveal that compacting with the piston already brings an improvement in the reaction, in the terms above discussed. This fact has sense if talking about solid reactions because compacting and heating provide an intimate contact between molecules with a higher contact surface area and thus enhance the reaction. On the other hand, working without compacting did not provide considerable improvement even if temperature was applied. Thus as explain above, the pressure was fixed at 150 MPa for further experiments, a value with higher yield and easier to handle.

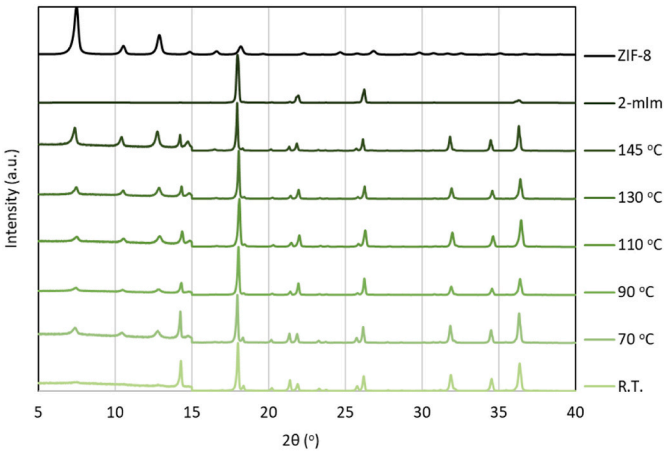

Fig. 3. XRD patterns of syntheses at different temperatures (run #1-#6 in Table 1). The intensity values from 5 to 15° in solventless syntheses were multiplied by 10.

3.4. Effect of the amount of promotor

To study the influence of promotor on the solventless synthesis of ZIF-8, a starting amount of 5 mg of NH_4NO_3 was used (0.8 wt%). Then, this amount was varied from 5 to 80 mg (0.8–11.6 wt%, runs #13 - #18 in Table 1). Yields to ZIF were calculated from the TGA curves in Fig. S6, where the highest yield (57.5%) was obtained for the sample with 40 mg (run #17 in Table 1). According to the characterization, above 15 mg of NH_4NO_3, two different products appeared, besides the expected ZIF-8, ZIF-L was evidenced (Fig. 4). ZIF-L is a two-dimensional layered ZIF structure constituted by the same building blocks that ZIF-8 [29]. ZIF-L is considered as a non-porous polymorph of ZIF-8. XRD pattern of NH_4NO_3 is also shown to check that the presence of the salt blended with the products. Thus if a loss weight appears at around 250 °C, corresponding to NH_4NO_3, it is inferred that part of the salt remained encapsulated on ZIF-8 porous. This agrees with the fact of ion inclusion in the porous ZIF structure, which would enhance and direct the ZIF synthesis [21]. XRD pattern of mIm is also shown in Fig. 4 to check the opposite: the lack of total reaction and, in consequence, the appearance of ligand impregnating the final product.

For samples with 40 and 80 mg of NH_4NO_3, the presence of ZIF-L is very important being majority at 40 mg, with its main peaks higher than those of ZIF-8, and exclusive at 80 mg. In sample with 40 mg of NH_4NO_3, the composition of the ZIF mixture was around 89.8% of ZIF-L, 7.8% of ZIF-8 and 2.4% of ZnO (calculated with MAUD: Material Analysis Using Diffraction software, Fig. S7 [30]). In most of the samples, washing procedure was not performed in order to show how products are achieved directly from the press (including unreacted compounds) and their correspondent yields. From the beginning, our objective was improving the yield of reaction but also trying to avoid the use of solvent. For that reason, undesired products were removed just in the most interesting sample, the one with the highest yield (40 mg of NH_4NO_3). In this sample, a method was carried out with a little amount of ethanol to convert ZIF-L into ZIF-8 as well as to remove all the unreacted compounds (Section 3.5.). It is worth mentioning that in the MAUD composition, the amount of ZnO seems to be lower than that obtained from TGA, overestimating the ZIF yield. This can be due to the fact that ZIF crystals, grown on ZnO particles, would interfere with the XRD radiation under estimating the amount of ZnO.

3.5. Conversion from ZIF-L to ZIF-8

With the purpose of studying the transformation of ZIF-L into ZIF-8, a first conversion was carried out in which 0.08 g of product was mixed with 8 mL of ethanol and heated at 60 °C for 72 h [31]. The conversion of ZIF-L into ZIF-8 with a little amount of solvent was reached easily as shown in the corresponding XRD patterns of Fig. 5. The empirical formula of ZIF-L was previously reported as $Zn(mlm)_2{\cdot}(HmIm)_{1/2}{\cdot}(H_2O)_{3/2}$ [29]. This means that half molecule of linker is not coordinated to Zn but trapped in the ZIF structure. Upon treatment with ethanol, the non-coordinated ligand disappears at the same time that ZIF-L is transformed into ZIF-8, in line with the TGA data collected in Fig. S8 (for both samples, with 40 and 80 mg of NH_4NO_3), where the step at ca. 250 °C, related to HmIm trapped in ZIF-L, practically disappears. Fig. 5 shows the diffraction patterns of the conversion for both samples, where XRD

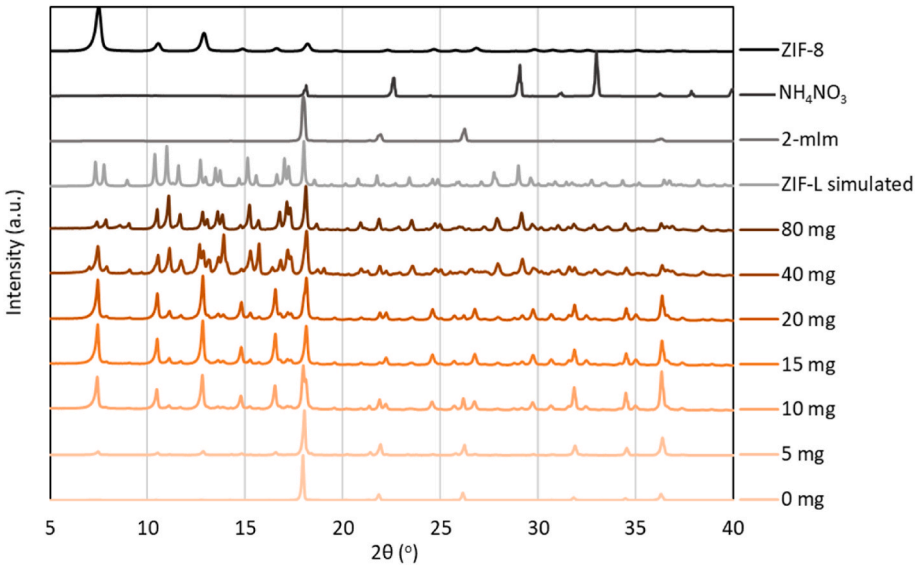

Fig. 4. XRD patterns of samples increasing the amount of NH_4NO_3 (run #4 and #13 - #18).

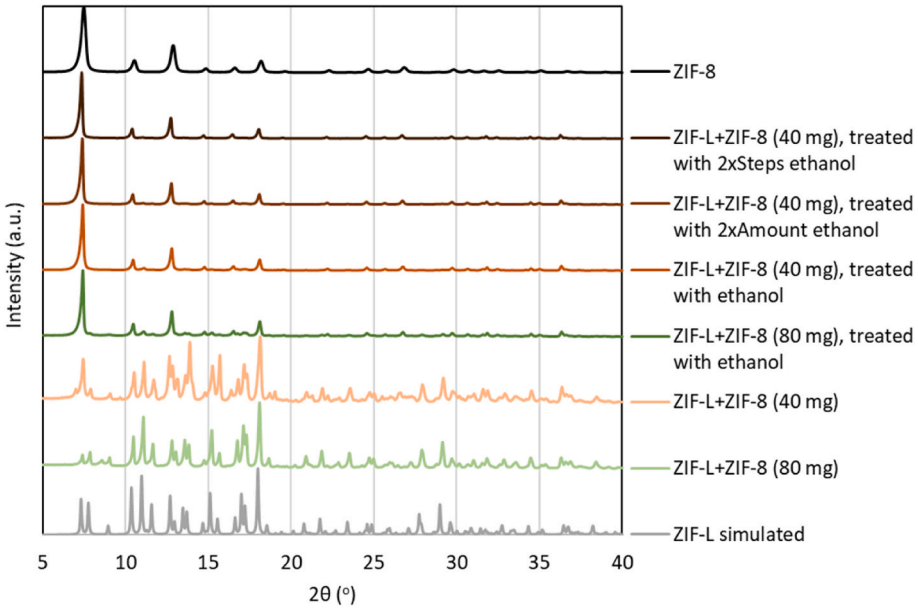

Fig. 5. Characterization of samples with 40 and 80 mg of NH_4NO_3 (in green and orange respectively) before and after treatment with ethanol. (For interpretation of the references to colour in this figure legend, the reader is referred to the Web version of this article.)

pattern of treated samples reveal similar intensities to ZIF-8, meaning that the conversion from ZIF-L to ZIF-8 was successful. For sample with 40 mg of NH_4NO_3 after treatment with ethanol, the percentage of conversion to ZIF-8 was calculated again by means of MAUD software. From a starting sample with 89.8% of ZIF-L, 7.8% of ZIF-8 and 2.4% of ZnO (as said before), the conversion revealed a mixture of 21.1% of ZIF-L, 71.7% of ZIF-8 and 7.2% of ZnO (Fig. S9). The increase of ZnO, when comparing its share before and after ZIF-L conversion, can be explained by the detachment of ZIF crystals from the ZnO surfaces as ZIF-L is transformed into ZIF-8. This would leave the ZnO particles more exposed to the XRD radiation.

To increase the yield of conversion from ZIF-L to ZIF-8, the same experiment was carried out with methanol, due to the higher solubility of mIm in this solvent. As for ethanol, all unreacted ligand was not completely dissolved in methanol and a little amount of it remained encapsulated in the ZIF structure. This is related to the slight step at ca. 250 °C in the TGA curve, corresponding to mIm in ZIF-L, shown in Fig. S10, where a comparison of conversion with both solvents is shown. MAUD software was used as well for calculating the composition of this product converted with methanol, providing a result of 65.2% of ZIF-8, 31.4% of ZIF-L and 3.4% of ZnO (Fig. S11).

As a considerable improvement was not achieved with methanol, two new conversion methods were performed based on ethanol (greener solvent than methanol [32]). One of them consists of following the same conversion procedure but with double amount of ethanol and the other consists of carrying out the same procedure in two steps (in series), both with the sample corresponding to 40 mg of NH_4NO_3. XRD patterns in Fig. 5 show the total conversion in terms of diffraction from an initial mixture of ZIF-L and ZIF-8 (89.8% of ZIF-L, 7.8% of ZIF-8 and 2.4% of ZnO, as said above) to ZIF-8. Yields to ZIF-8 of 55.8% and 58.2% were obtained in the treatment with double amount of ethanol and two steps, respectively (calculated from the TGA curves in Fig. S12a and as

explained in the experimental section). MAUD software was used for calculating the composition of both products (Figs. S12b and c). Fig. 6 shows the composition (in percentage) of ZIF-8, ZIF-L and ZnO for the initial synthesis with 40 mg of NH_4NO_3 and the products obtained with each conversion method.

3.6. Effect of reaction time

Different reaction times were studied while maintaining constant the parameters optimized previously, i.e. 110 °C and 150 MPa, and studied for 15 mg and 40 mg of NH_4NO_3 (in Table 1, runs #25 - #31 and #19 - #24, respectively). Both samples were chosen because the first one is that with the highest yield for the synthesis of just ZIF-8 (in absence of ZIF-L phase), while the second one corresponds to the highest yield of the synthesis, ZIF-L being the main product. As shown in Table 1, the highest yield for 40 mg of NH_4NO_3 was obtained for 10 min of reaction time, achieving a value of 57.5%. It has to be taken into account that this yield is mainly conversion to ZIF-L. The highest yield before appearing ZIF-L would be with 15 mg of NH_4NO_3 with a value of 40.2% also for 10 min of reaction time. TGA data used to calculate yield are in Fig. S13 (for samples with 15 mg of NH_4NO_3) and S14 (for samples with 40 mg of NH_4NO_3). Fig. 7 and Fig. 8 show XRD patterns of samples with 15 and 40 mg of NH_4NO_3, respectively, which confirm that from the first minute the reaction takes place.

3.7. Effect of mIm/Zn molar ratio

The last parameter studied was the ligand:metal molar ratio, starting from the stoichiometric ratio inspired by the empirical formula of ZIF-8 ($Zn(mIm)_2$) and increasing the amount of 2-mIm until a 3:1 ratio. It was thought that an increase in the mIm/Zn ratio would increase the reaction yield because maybe some ligand could remain in the pores and do not react with ZnO. We studied for both samples, 15 and 40 mg of NH_4NO_3, looking for an improve of the synthesis of just ZIF-8 (15 mg) and for the synthesis with highest yield (40 mg) even if it was a mixture of ZIFs. As shown in Table 1, the highest yield was achieved with the stoichiometric amount for both cases, 15 and 40 mg of NH_4NO_3 (run #32 with 57.5% and run #35 with 40.2%, respectively). TGA curves and XRD patterns are shown in Fig. S15 (for samples with 15 mg of NH_4NO_3) and S16 (for samples with 40 mg of NH_4NO_3).

Electron microscopy was performed in order to elucidate the size and shape of the ZIF crystals that we obtained. Fig. 9a and b shows SEM images for samples with different amount of NH_4NO_3 neither washed nor activated. In Fig. 9a, sample with 5 mg of NH_4NO_3 is shown, where there is no clear evidence of ZIF-8 crystals, even if the XRD characterization suggested some yield to ZIF. Sample with 40 mg of NH_4NO_3 is

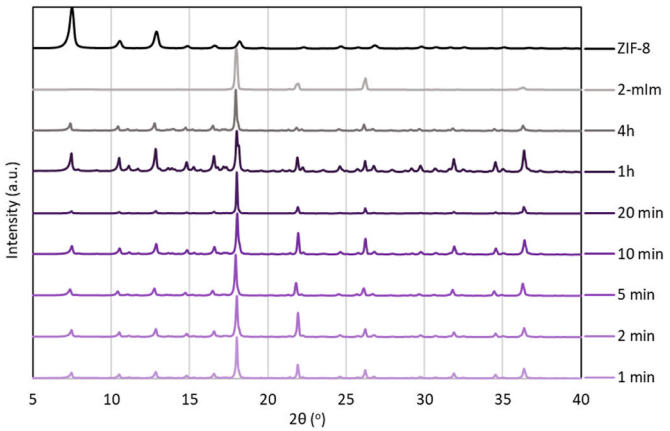

Fig. 7. *XRD patterns for different reaction times, at 110 °C and* 150 MPa, *in a sample with* 15 mg *of* NH_4NO_3.

depicted in Fig. 9b, where the two-dimensional layered ZIF-L structure predominates. Fig. 9c and d collect images of samples after treatment with ethanol, with double amount of solvent and two steps of treatment, respectively. This reveals the conversion of samples with 40 mg of NH_4NO_3 (Fig. 9b) into ZIF-8, showing the characteristic rombododecahedral growth habit of this MOF. Samples after treatment with double amount of ethanol and with two steps of ethanol exhibited particle sizes of 205 ± 90 nm and 243 ± 110 nm, respectively. Histograms of both samples are collected in Figs. S17a and S17b. Finally, Fig. S18 shows the results of the SEM observation corresponding to the first conversion with ethanol, where the product did not reveal the ZIF-8 morphology as defined as with double amount of solvent and two steps of treatment with ethanol. For comparison, SEM images of ZnO and ZIF-8 (synthesized by solvothermal method with methanol) are shown in Fig. S19.

Nitrogen adsorption−desorption isotherms were achieved and specific surface areas were calculated by the BET method. The values are collected in Table S1 and Fig. 10, for samples with different amount of NH_4NO_3, for samples converted to ZIF-8 in presence of alcohol and for samples obtained from initial solid mixtures with different L/M ratios. BET specific surface area increases from 5 to 15 mg of NH_4NO_3 samples, but it starts to decrease above 20 mg, due to the appearance of ZIF-L phase, which has lower surface area because of its dense laminar structure. Samples with 40 mg of NH_4NO_3 after treatment with ethanol present an increase in the BET specific surface area by 10 times. Transformation with methanol did not produce an increase in the solubility of the ligand, which is shown in the lower BET specific surface area. This fact could be associated to the encapsulation of the ligand in

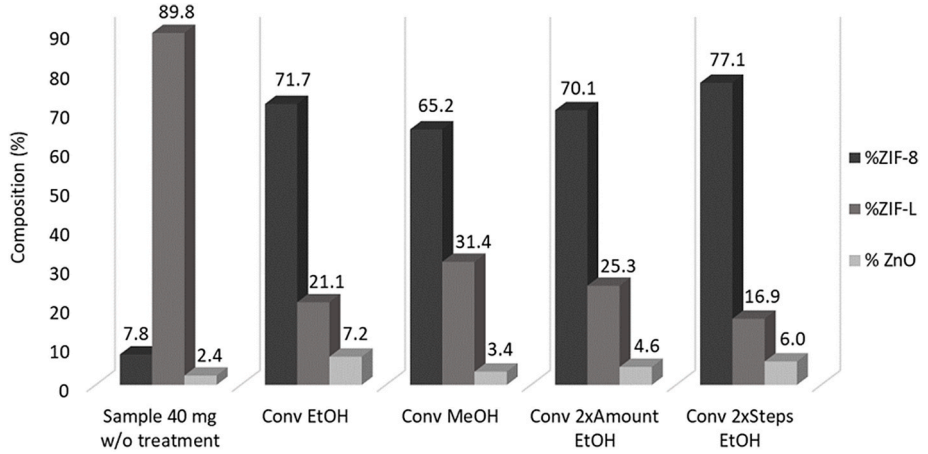

Fig. 6. MAUD estimations of compositions in percentage of the initial sample of 40 mg of NH_4NO_3 and the samples after treatments.

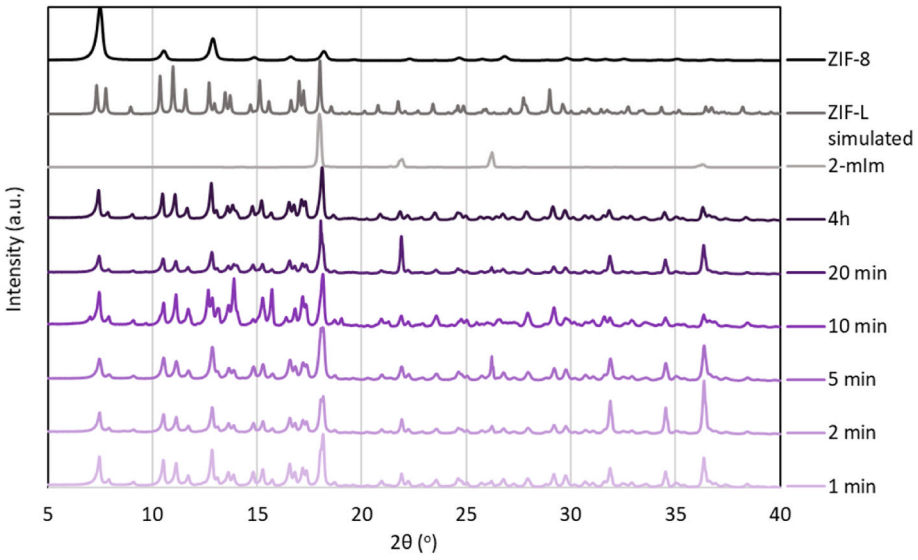

Fig. 8. XRD patterns for different reaction times, at 110 °C and 150 MPa, in a sample with 40 mg of NH_4NO_3.

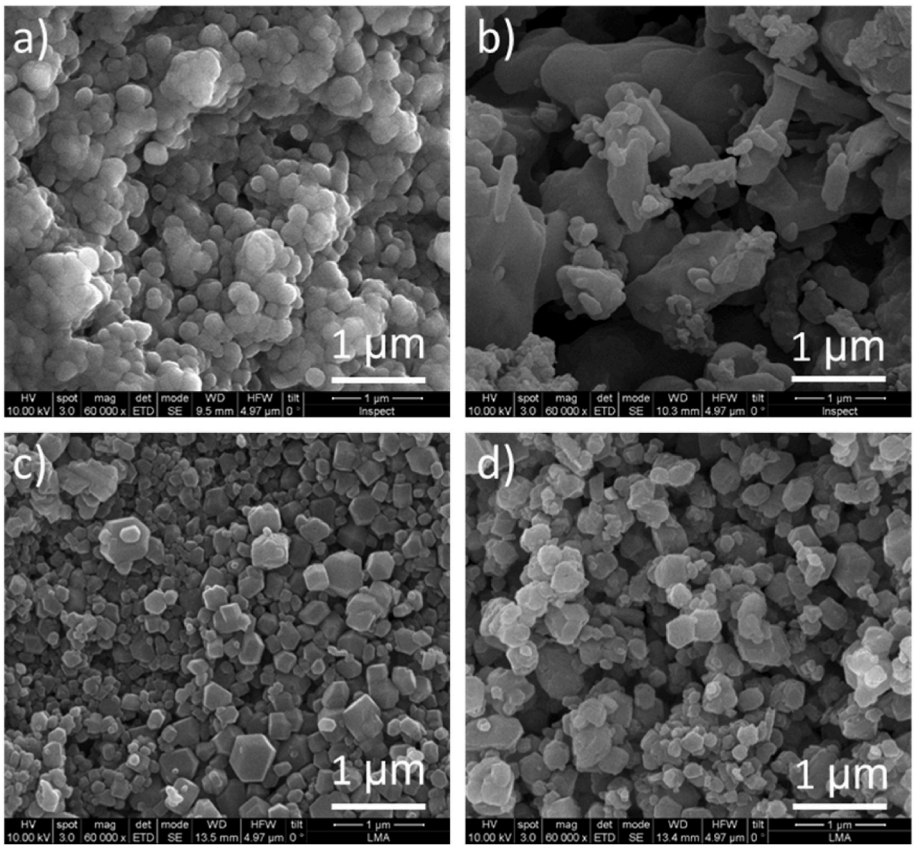

Fig. 9. SEM images for samples obtained at 110 °C and 150 MPa with: a) 5 mg of NH_4NO_3, b) 40 mg of NH_4NO_3, c) after treatment with double amount of ethanol and d) after treatment with two steps of ethanol.

ZIF-8 porosity as explained before. Moreover, the conversion carried out with double amount of ethanol and two steps of treatment provided the highest BET specific surface area values (860 ± 16 and 947 ± 17 m^2/g, respectively) near to the value obtained for ZIF-8 after submitting it to press conditions (1047 ± 19 m^2/g). These values below the one corresponding to pure ZIF-8 (1730 m^2/g) is in line with the fact that the TGA yields are more representative of the evolution of the reaction than the MAUD calculations, based on XRD measurements where ZIFs would shield ZnO particles. This suggests in turn the generation of core-shell morphologies.

Once it has been demonstrated that an increase in the reaction yield for the synthesis of ZIF-8 and ZIF-L is possible, future work will be directed to extrapolate this method to the synthesis of other ZIFs such as ZIF-94 and ZIF-7 or ZIF-11, for example.

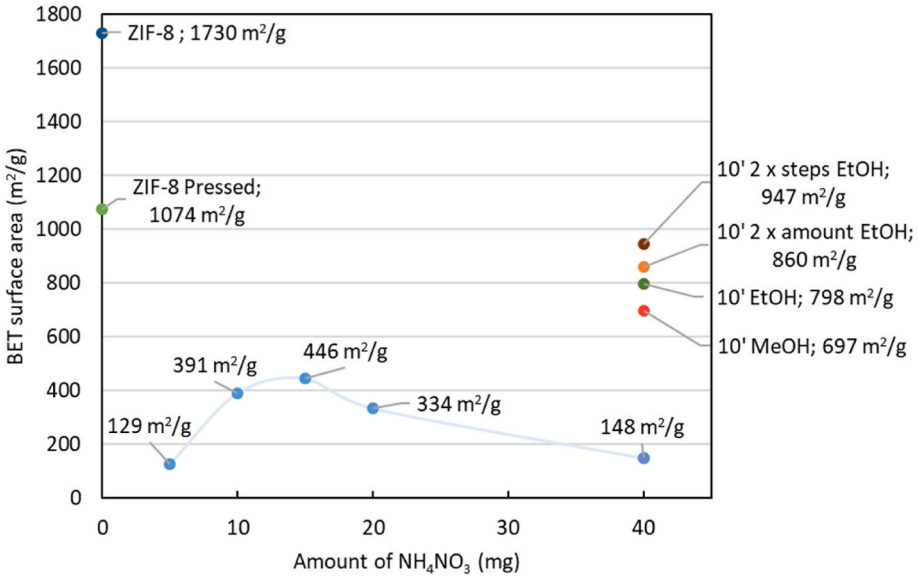

Fig. 10. BET specific surface area values of samples with different amount of NH_4NO_3 and after the alcohol conversion treatment from ZIF-L to ZIF-8.

4. Conclusion

In conclusion, an improvement of the reaction yield for the high pressure synthesis of ZIF-8 has been achieved by working at temperatures above the room one. The optimization of reaction conditions such as temperature, reaction time and the amount of promotor added to the reaction concluded in products with higher yield even being characterized without washing or activating processes. It was demonstrated that from the first minute, the reaction took place and products were formed, which could be interesting for a future industrial implementation.

According to the addition of promotor, 15 mg of NH_4NO_3 provided the highest yield for the synthesis of crystalline (as stated by XRD) ZIF-8. Above this amount, two phases, ZIF-L and ZIF-8, were obtained as product, ZIF-L being predominant in samples with 40 and 80 mg of promotor. For these samples, which reached the highest yield to ZIF, a very little amount of solvent (ethanol) was used for the conversion of ZIF-L into ZIF-8. The analysis of the BET specific surface area revealed a highest value of 947 m^2/g upon proper conversion of ZIF-L into ZIF-8 with two sequential treatments with ethanol. This value is close to that measured when conventional ZIF-8 was submitted to high temperature and pressure conditions (1074 m^2/g at 110 °C and 150 MPa for 10 min). Structure refinements using software MAUD allowed the calculation of ZIF-L/ZIF-8/ZnO relative amounts underestimating the amount of ZnO due to the formation of core-shell particles in which the ZIFs would shield the ZnO.

Future work in line with this article could be related to the extrapolation of this method to the synthesis of other MOFs or even COFs and the possibility of scaling it up for industrial applications.

CRediT authorship contribution statement

Marta Pérez-Miana: Conceptualization, Methodology, Validation, Formal analysis, Investigation, Writing – original draft, Writing – review & editing, Visualization. **Javier U. Reséndiz-Ordóñez:** Methodology, Validation, Formal analysis, Investigation, Writing – original draft. **Joaquín Coronas:** Conceptualization, verification, Writing – original draft, Writing – review & editing, Funding acquisition, Supervision.

Declaration of competing interest

The authors declare that they have no known competing financial interests or personal relationships that could have appeared to influence the work reported in this paper.

Acknowledgements

Financial support from the Research Projects MAT2016-77290-R and the PID2019-104009RB-I00/AEI/10.13039/501100011033 (Spanish AEI/FEDER, UE), the Aragón Government (T43-20R and Marta Pérez-Miana PhD grant) and the ESF are gratefully acknowledged. All the microscopy work was done in the Laboratorio de Microscopías Avanzadas (LMA). The authors acknowledge the LMA for offering access to their instruments and expertise and the Servicios de Apoyo a la Investigación (SAI), both from the Universidad de Zaragoza.

Appendix A. Supplementary data

Supplementary data to this article can be found online at https://doi.org/10.1016/j.micromeso.2021.111487.

References

[1] Q. Wang, D. Astruc, State of the art and prospects in metal–organic framework (MOF)-Based and MOF-derived nanocatalysis, Chem. Rev. 120 (2020) 1438–1511, https://doi.org/10.1021/acs.chemrev.9b00223.
[2] T. Ghanbari, F. Abnisa, W.M.A. Wan Daud, A review on production of metal organic frameworks (MOF) for CO2 adsorption, Sci. Total Environ. 707 (2020), 135090, https://doi.org/10.1016/j.scitotenv.2019.135090.
[3] O.K. Farha, A. Özgür Yazaydın, I. Eryazici, C.D. Malliakas, B.G. Hauser, M. G. Kanatzidis, S.T. Nguyen, R.Q. Snurr, J.T. Hupp, De novo synthesis of a metal–organic framework material featuring ultrahigh surface area and gas storage capacities, Nat. Chem. 2 (2010) 944–948, https://doi.org/10.1038/nchem.834.
[4] H. Li, M. Eddaoudi, M. O'Keeffe, O.M. Yaghi, Design and synthesis of an exceptionally stable and highly porous metal-organic framework, Nature 402 (1999) 276–279, https://doi.org/10.1038/46248.
[5] Z. Ji, H. Wang, S. Canossa, S. Wuttke, O.M. Yaghi, Pore chemistry of metal–organic frameworks, Adv. Funct. Mater. 30 (2020), 2000238, https://doi.org/10.1002/adfm.202000238.
[6] H. Li, L. Li, R.-B. Lin, W. Zhou, Z. Zhang, S. Xiang, B. Chen, Porous metal-organic frameworks for gas storage and separation: status and challenges, EnergyChem 1 (2019), 100006, https://doi.org/10.1016/j.enchem.2019.100006.
[7] J.L.C. Rowsell, O.M. Yaghi, Strategies for hydrogen storage in metal-organic frameworks, Angew. Chem. Int. Ed. 44 (2005) 4670–4679, https://doi.org/10.1002/anie.200462786.
[8] F. Cacho-Bailo, G. Caro, M. Etxeberría-Benavides, O. Karvan, C. Téllez, J. Coronas, High selectivity ZIF-93 hollow fiber membranes for gas separation, Chem. Commun. 51 (2015) 11283–11285, https://doi.org/10.1039/C5CC03937A.
[9] S. Sorribas, P. Gorgojo, C. Téllez, J. Coronas, A.G. Livingston, High flux thin film nanocomposite membranes based on metal–organic frameworks for organic

solvent nanofiltration, J. Am. Chem. Soc. 135 (2013) 15201–15208, https://doi.org/10.1021/ja407665w.
[10] Y. Sun, L. Zheng, Y. Yang, X. Qian, T. Fu, X. Li, Z. Yang, H. Yan, C. Cui, W. Tan, Metal–organic framework nanocarriers for drug delivery in biomedical applications, Nano-Micro Lett. 12 (2020) 103, https://doi.org/10.1007/s40820-020-00423-3.
[11] L. Paseta, G. Potier, S. Abbott, J. Coronas, Using Hansen solubility parameters to study the encapsulation of caffeine in MOFs, Org. Biomol. Chem. 13 (2015) 1724–1731, https://doi.org/10.1039/C4OB01898B.
[12] L. Paseta, E. Simón-Gaudó, F. Gracia-Gorría, J. Coronas, Encapsulation of essential oils in porous silica and MOFs for trichloroisocyanuric acid tablets used for water treatment in swimming pools, Chem. Eng. J. 292 (2016) 28–34, https://doi.org/10.1016/j.cej.2016.02.001.
[13] E.E. Sann, Y. Pan, Z. Gao, S. Zhan, F. Xia, Highly hydrophobic ZIF-8 particles and application for oil-water separation, Separ. Purif. Technol. 206 (2018) 186–191, https://doi.org/10.1016/j.seppur.2018.04.027.
[14] Z. Lai, Development of ZIF-8 membranes: opportunities and challenges for commercial applications, Curr. Opin. Chem. Eng. 20 (2018) 78–85, https://doi.org/10.1016/j.coche.2018.03.002.
[15] N. Liédana, A. Galve, C. Rubio, C. Téllez, J. Coronas, CAF@ZIF-8: one-step encapsulation of caffeine in MOF, ACS Appl. Mater. Interfaces 4 (2012) 5016–5021, https://doi.org/10.1021/am301365h.
[16] A. Noguera-Díaz, N. Bimbo, L.T. Holyfield, I.Y. Ahmet, V.P. Ting, T.J. Mays, Structure–property relationships in metal-organic frameworks for hydrogen storage, Colloid. Surface. Physicochem. Eng. Aspect. 496 (2016) 77–85, https://doi.org/10.1016/j.colsurfa.2015.11.061.
[17] W. Xue, Q. Zhou, F. Li, B.S. Ondon, Zeolitic imidazolate framework-8 (ZIF-8) as robust catalyst for oxygen reduction reaction in microbial fuel cells, J. Power Sources 423 (2019) 9–17, https://doi.org/10.1016/j.jpowsour.2019.03.017.
[18] K. Kida, M. Okita, K. Fujita, S. Tanaka, Y. Miyake, Formation of high crystalline ZIF-8 in an aqueous solution, CrystEngComm 15 (2013) 1794, https://doi.org/10.1039/c2ce26847g.
[19] L.S. Lai, Y.F. Yeong, K.K. Lau, A.M. Shariff, Effect of synthesis parameters on the formation of ZIF-8 under microwave-assisted solvothermal, Procedia Eng 148 (2016) 35–42, https://doi.org/10.1016/j.proeng.2016.06.481.
[20] B. Seoane, J.M. Zamaro, C. Tellez, J. Coronas, Sonocrystallization of zeolitic imidazolate frameworks (ZIF-7, ZIF-8, ZIF-11 and ZIF-20), CrystEngComm 14 (2012) 3103–3107, https://doi.org/10.1039/c2ce06382d.
[21] S. Tanaka, K. Kida, T. Nagaoka, T. Ota, Y. Miyake, Mechanochemical dry conversion of zinc oxide to zeolitic imidazolate framework, Chem. Commun. 49 (72) (2013) 7884–7886, https://doi.org/10.1039/C3CC43028F.
[22] L. Paseta, G. Potier, S. Sorribas, J. Coronas, Solventless synthesis of MOFs at high pressure, ACS Sustain. Chem. Eng. 4 (2016) 3780–3785, https://doi.org/10.1021/acssuschemeng.6b00473.
[23] A.J. Graham, D.R. Allan, A. Muszkiewicz, C.A. Morrison, S.A. Moggach, The effect of high pressure on MOF-5: guest-induced modification of pore size and content at high pressure, Angew. Chem. Int. Ed. 50 (2011) 11138–11141, https://doi.org/10.1002/anie.201104285.
[24] S.A. Moggach, T.D. Bennett, A.K. Cheetham, The effect of pressure on ZIF-8: increasing pore size with pressure and the formation of a high-pressure phase at 1.47 GPa, Angew. Chem. Int. Ed. 48 (2009) 7087–7089, https://doi.org/10.1002/anie.200902643.
[25] R. Monteagudo-Olivan, L. Paseta, G. Potier, P. López-Ram-de-Viu, J. Coronas, Solvent-free encapsulation at high pressure with carboxylate-based MOFs: solvent-free encapsulation at high pressure with carboxylate-based MOFs, Eur. J. Inorg. Chem. 2019 (2019) 29–36, https://doi.org/10.1002/ejic.201800985.
[26] S. Tanaka, T. Nagaoka, A. Yasuyoshi, Y. Hasegawa, J.F.M. Denayer, Hierarchical pore development of ZIF-8 MOF by simple salt-assisted mechanosynthesis, Cryst. Growth Des. 18 (2018) 274–279, https://doi.org/10.1021/acs.cgd.7b01211.
[27] M. Taheri, I.D. Bernardo, A. Lowe, D.R. Nisbet, T. Tsuzuki, Green full conversion of ZnO nanopowders to well-dispersed zeolitic imidazolate framework-8 (ZIF-8) nanopowders via a stoichiometric mechanochemical reaction for fast dye adsorption, Cryst. Growth Des. 20 (2020) 2761–2773, https://doi.org/10.1021/acs.cgd.0c00129.
[28] T. Friščić, I. Halasz, P.J. Beldon, A.M. Belenguer, F. Adams, S.A.J. Kimber, V. Honkimäki, R.E. Dinnebier, Real-time and in situ monitoring of mechanochemical milling reactions, Nat. Chem. 5 (2013) 66–73, https://doi.org/10.1038/nchem.1505.
[29] R. Chen, J. Yao, Q. Gu, S. Smeets, C. Baerlocher, H. Gu, D. Zhu, W. Morris, O. M. Yaghi, H. Wang, A two-dimensional zeolitic imidazolate framework with a cushion-shaped cavity for CO2 adsorption, Chem. Commun. 49 (2013) 9500–9502, https://doi.org/10.1039/c3cc44342f.
[30] L. Lutterotti, Total pattern fitting for the combined size–strain–stress–texture determination in thin film diffraction, Nucl. Instrum. Methods Phys. Res. B: Beam Interact. Mater. At. 268 (2010) 334–340, https://doi.org/10.1016/j.nimb.2009.09.053.
[31] Z.-X. Low, J. Yao, Q. Liu, M. He, Z. Wang, A.K. Suresh, J. Bellare, H. Wang, Crystal transformation in zeolitic-imidazolate framework, Cryst. Growth Des. 14 (2014) 6589–6598, https://doi.org/10.1021/cg501502r.
[32] C. Capello, U. Fischer, K. Hungerbühler, What is a green solvent? A comprehensive framework for the environmental assessment of solvents, Green Chem. 9 (2007) 927–934, https://doi.org/10.1039/b617536h.